Magnetic-order induced effects in nanocrystalline NiO probed by Raman spectroscopy

Nisha Bala,[1] H. K. Singh,[2] Shikha Verma,[3] and Shyama Rath[1,*]

[1]*Department of Physics and Astrophysics, University of Delhi, Delhi 110007, India*

[2]*National Physical Laboratory, Dr. K S Krishnan Marg, New Delhi, Delhi 110012, India*

[3]*Institue of Physics, P.O.: Sainik School, Bhubaneswar - 751005, Bhubaneswar, India*

(Received 19 May 2020; revised 19 June 2020; accepted 2 July 2020; published 16 July 2020)

The magnetic-order induced effects in nanocrystalline NiO are investigated through the phonons and magnons observed in the Raman spectra. The key observations are (i) an anisotropy of the first-order transverse and longitudinal optical phonons, with a splitting on the order of 5 meV and (ii) a marked size and excitation wavelength variation of the two-magnon peak, which varies linearly with a redshift of $\sim$50 cm^{-1} with a size reduction from 105 to 30 nm. The magnon-related peaks, in contrast to the phonons, are suppressed for near-resonance laser excitations. The experimental results are interpreted in terms of the exchange interactions and strong electron-electron correlations. The magnetization measurements shows a crossover to ferromagnetism with large coercivities and magnetization with decreasing size, which is shown to be due to the thermoinduced contribution.

DOI: 10.1103/PhysRevB.102.024423

I. INTRODUCTION

NiO is antiferromagnetically ordered below its Néel temperature (T_N) of 523 K, with the ordering arising out of alternating ferromagnetically aligned (111) planes that are antiferromagnetically aligned with respect to each other, and with the direction of spin alignment within each plane being accepted to be along $\langle 112 \rangle$. A transition from an antiferromagnetic behavior in the bulk to a ferromagnetic one when the size is reduced to nanometric scales makes nanometric NiO an interesting material for both ferromagnetic and antiferromagnetic (AFM) spintronics [1–3]. While spintronics conventionally relies on means to manipulate the magnetic moment of ferromagnets, antiferromagnet spintronics, which exploits the magnetic properties of antiferromagnets for their use as alternate components of spintronic devices, has been an emerging area. Understanding the size-dependent magnetization is useful both for practical applications as well as to elucidate the structure-properties correlation in antiferromagnetic oxide nanostructures. Towards this, Raman spectroscopy is a sensitive tool to probe the magnetic behavior at the microscopic level.

NiO (like MnO) presents itself as a benchmark material for a fundamental understanding of strongly correlated systems. The strong correlations arise from the Coulomb repulsions between the 3*d* electrons on the Ni ions lead to AFM ordering and a concomitant structural distortion, albeit minor ($<10^{-3}$), below the Néel temperature from a cubic rocksalt structure to a rhombohedral structure with a distortion along the $\langle 111 \rangle$ direction. However, early theoretical treatments of the lattice dynamical properties were based on shell-model calculations [4–6] and Hartree-Fock approximation [7] and neglected the effects of electron correlations. Experimental neutron-scattering studies [4,5] of the phonon spectrum were also accordingly interpreted.

Subsequent theoretical studies have however emphasized the important role of correlations in the lattice dynamics of transition-metal oxides. Massidda *et al.* [8], using *ab initio* and model calculations, proposed that the AFM ordering arising due to the strong correlation between the *d* electrons can lead to an anisotropy of the nonmagnetic properties such as the lattice dynamics. The magnetic-order induced splitting of the zone-center transverse optical (TO) phonon was estimated to be on the order of about 10% of its energy in MnO and was proposed to be similar in NiO. Experimental investigation of the first-order TO phonon anisotropy by neutron scattering [9] (possibly the only study) validated the predictions of Ref. [8]. It is however noteworthy that the magnitude of the phonon splitting ($\sim$5 meV) was the same for both NiO and MnO, despite a much smaller distortion angle (0.07°) as compared to MnO (0.6°). The TO phonon splitting reported in inelastic x-ray scattering experiments [10] was much smaller and interpreted in terms of an anisotropic polarization. Savrasov *et al.* [11] incorporated strong correlations by merging the local density approximation of the density-functional theory (DFT) with the dynamical mean-field theory. The values of the optical frequencies and the calculated LO-TO splitting agreed with Ref. [5], but differed from Ref. [4]. However, no anisotropy in the phonons was predicted. Luo *et al.* [12] introduced correlations through a Hubbard correction U to the local spin-density approximation method and determined the splitting to depend on the coupling of the phonons to J_1. While the calculated phonon splitting also agrees well with Ref. [5] for MnO, it is underestimated ($\sim$1.8 meV) for NiO. The inclusion of a Hubbard parameter to the generalized gradient approximation (GGA) of the DFT Hamiltonian in Ref. [13] led to an upshift of the phonon frequencies and also deduced a splitting in both the TO and LO phonons. Wang *et al.* [14] found an almost negligible splitting by combining

*srath@physics.du.ac.in

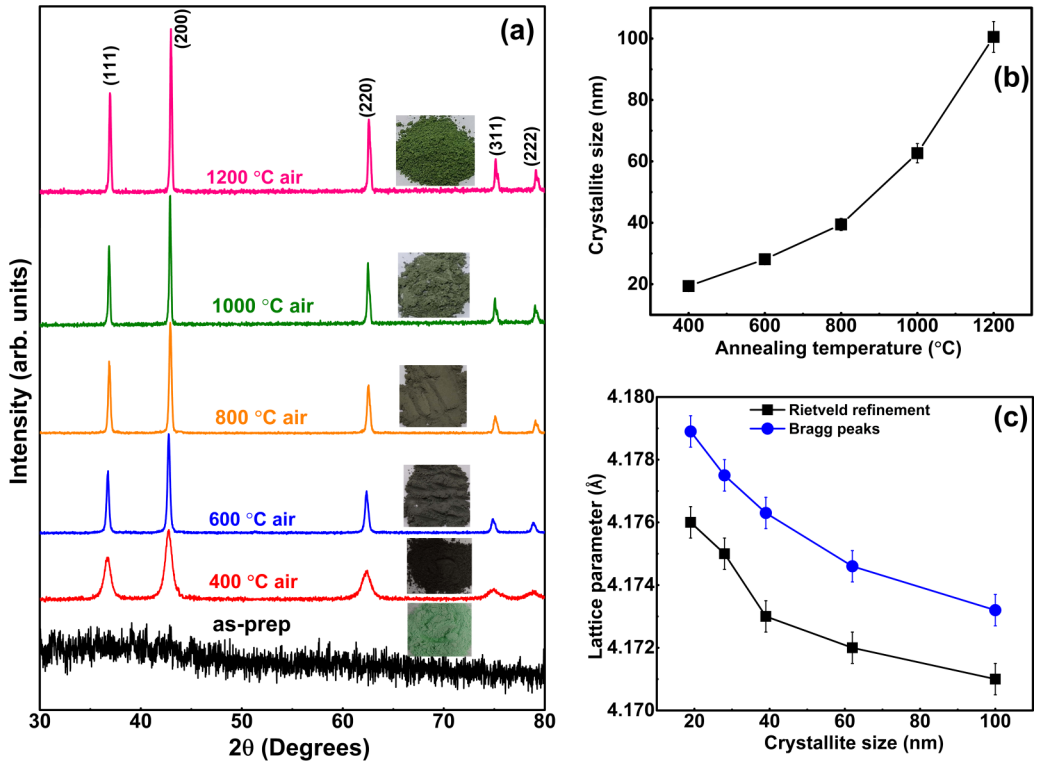

FIG. 1. (a) XRD patterns of thermally annealed NiO samples in air atmosphere, (b) variation of crystallite size with annealing temperature, and (c) variation of lattice parameter with crystallite size. The solid lines are a guide to the eye.

the effects of the deviation from ideal cubic symmetry and the strong correlations and inferred it to be due to the weaker anisotropy of the electronic response in NiO as compared to MnO. Aytan *et al.* showed a splitting of both the TO and LO phonons through DFT calculations, and have reported the Raman spectra as well [15]. In general, Raman investigations of the phonon spectra of NiO have been sparse [15–18]. The aforementioned observations thus warrant a larger body of experimental evidence of the phonon spectrum of NiO and provide the motivation for our studies and as summarized in Ref. [8]: "Such a splitting and its anisotropy are possibly hidden in the experimental spectra of MnO and NiO, and should prompt further experimental verification below T_N in both materials."

The two-magnon (2M) mode in the Raman spectra, whose occurrence is associated with a signature of AFM ordering, provides a very useful probe of magnetic order. It has been investigated theoretically as well as experimentally through neutron scattering and Raman spectroscopy [15–26]. Its energy is related to the strength of the exchange interactions. The predominant interaction is the antiferromagnetic exchange J_2 between next-nearest neighbors, which are linked by a 180° Ni^{+2}-O^{-2}-Ni^{+2} superexchange path. The nearest-neighbor interaction, linked by a 90° Ni^{+2}-O^{-2}-Ni^{+2} path, is far weaker and is ferromagnetic. The magnetic as well as electronic and vibrational properties are influenced by the exchange interactions in NiO. The temperature dependence of this mode has been used to estimate the spin-phonon coupling [15].

In this study, we use high-resolution Raman spectroscopy to probe the phonon anisotropy and the finite-size effect on the two-magnon peak in NiO nanoparticles, which show an antiferromagnetic-ferromagnetic transition. The NiO nanoparticles investigated here were synthesized by a simple and cost-effective sol-gel method easily realizable in modest laboratories and producing a high yield of nanoparticles**.**

II. EXPERIMENTAL DETAILS

In the synthesis involving a sol-gel process, 0.5 M of the precursor, nickel acetate was added to 60 ml of methanol and stirred vigorously at 60 °C for 1 h, followed by oven drying at 100 °C for 24 h. The dried powder was annealed in a tubular furnace at various temperatures between 400 and 1200 °C in an air atmosphere. The NiO nanopowders showed distinct color changes due to stoichiometric changes, as shown in Fig. 1, varying from black to gray to greenish gray and finally green with the increase in annealing temperature. The light-green color of the as-prepared powder is due to $Ni(OH)_2$. The x-ray-diffraction (XRD) patterns were recorded in the 2θ range $20 - 80°$ at a rate of 2°/min with a Rigaku Ultima IV x-ray diffractometer with a Cu K_α source ($\lambda = 1.5418$ Å). A Ni filter for Cu K_β radiation has been used. Raman-scattering measurements were performed in a backscattering geometry at room temperature using an inVia Renishaw micro-Raman system equipped with a grating of 2400 lines/mm and a confocal microscope with a 50× objective. A 514-nm excitation wavelength was used and the scattered signal was recorded with a Peltier cooled charge-coupled device detector. A low incident laser power of 1 mW was used to avoid sample heating effects. A Horiba Jobin Yvon spectrometer (model T64000) equipped with a 325-nm excitation was

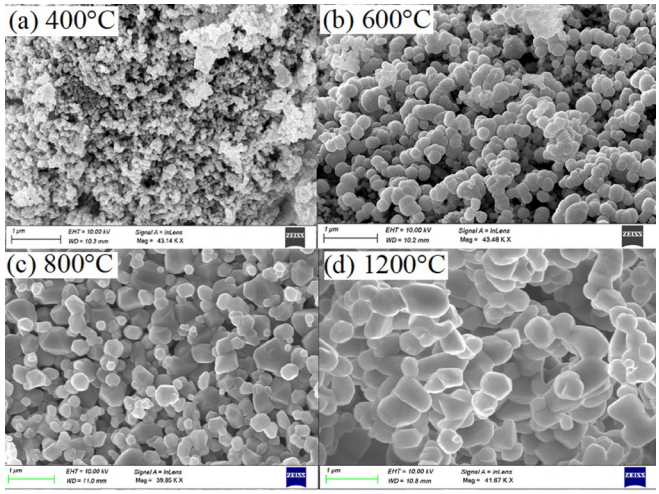

FIG. 2. FESEM images of NiO nanoparticles annealed at different temperatures:(a) 400 °C, (b) 600 °C, (c) 800 °C, and (d) 1200 °C.

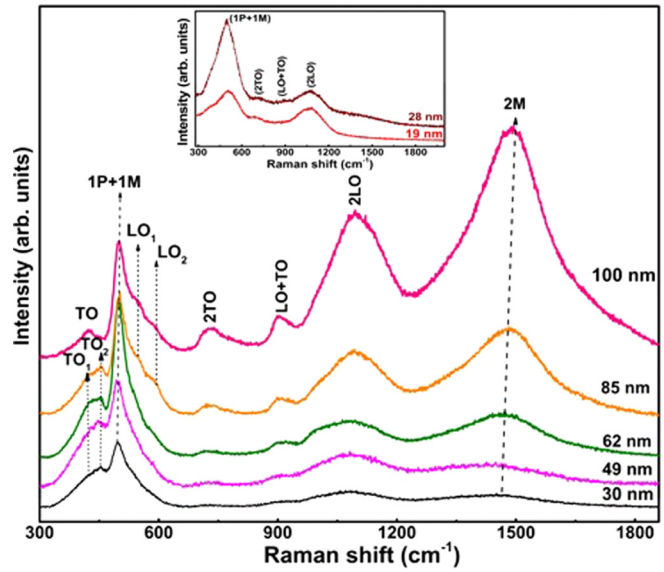

FIG. 3. Raman spectra of NiO nanoparticles showing the various modes as labeled. The splitting of the TO and LO modes are denoted as TO_1, TO_2 and LO_1, LO_2, respectively.

also used to record the Raman spectra. A JEOL MIRA3 LMH system was used for field-emission scanning electron microscopy (FESEM) measurements. Magnetic properties at room temperature were characterized by using a vibrating sample magnetometer (Lakeshore-VSM 7410) and the saturation magnetization (M_s) was extracted from the measured magnetic hysteresis (M-H) loops.

III. RESULTS AND DISCUSSION

Figure 1(a) shows the XRD patterns of the thermally annealed NiO powders. The observed diffraction peaks are indexed to the (1 1 1), (2 0 0), (2 2 0), (3 1 1), and (2 2 2) planes of the face-centered cubic structure of NiO in agreement with the standard [JCPDS file 00-001-1239]. The crystallite size (D) and strain (ε) values are estimated from the Williamson-Hall (W-H) method, using the expression $\beta\cos\theta = \frac{K\lambda}{D} + 4\sin\theta$, where D is the crystallite size, K is the shape factor, λ is the Cu K_α radiation wavelength, β is the full width at half maximum of the diffraction peak, and θ is the diffraction angle. The average crystallite size (D) ranges from 19 to 100 nm for an annealing temperature varying between 400 and 1200 °C, as shown in Fig. 1(b). Further, a Rietveld refinement of the x-ray diffractograms has been undertaken using the FULLPROF suite software. The peak shapes were modeled using pseudo-Voigt functions and the background was modeled using an interpolation of linear polynomials. The variation of the lattice parameters with crystallite size obtained from the Bragg peaks and Rietveld analyses are presented in Fig. 1(c).

Figure 2 shows the FESEM images of the NiO nanoparticles annealed at different temperatures. The surface morphology for the 400 and 600 °C annealed powders reveals the formation of well-separated and uniformly distributed spherical nanoparticles which resulted after the dehydration of the precipitate. For higher annealing temperatures, there is a tendency towards agglomeration. The particle-size distribution was obtained from the micrographs using IMAGEJ software. The shortest diameter of the particles is taken as an estimate of size. The average particle sizes are ∼22, 30, 44, and 104 nm for annealing temperatures of 400, 600, 800, and 1200 °C respectively. The values and the trend with annealing temperature are in good agreement with the same determined from the XRD data.

The Raman spectra of NiO nanoparticles are shown in Fig. 3. The first-order TO and LO phonons, which are forbidden for the rocksalt crystal structure of bulk NiO, are activated by the weak rhombohedral lattice distortion below T_N (R-3m structure) or due to defects. The spectrum is dominated by a broad asymmetric band at ∼500 cm^{-1}, labeled as (1P + 1M) band attributed to scattering by one-phonon (TO ∼450 cm^{-1}) and one-magnon (1M) ∼40 cm^{-1} excited simultaneously at the Brillouin-zone center [18]. The mode becomes sharper and intense with an increase in the crystallite size. The optical phonons show a clear splitting: the TO phonons are depicted as TO_1 and TO_2 and the LO phonon by LO_1 and LO_2. For lower annealing temperatures (and particle sizes), the larger width of the 1P + 1M obstructed the identification of the TO and LO peaks (inset of Fig. 2).

The peak positions of the split phonons are extracted by a deconvolution shown in Fig. 4(a) and plotted in Fig. 4(b) as a function of particle size. The positions of TO_1 and TO_2 are around 415 − 421 cm^{-1} (51.4–52.2 meV) and 455 − 459 cm^{-1} (56.3–56.8 meV), with a splitting $\Delta_{TO} = 4.9 - 4.6$ meV, which is comparable to the predicted splitting of 10% by Massidda *et al.* [8]. The only other comparison with experiments is with the TO_1 and TO_2 at 45 and 50 meV in neutron-scattering studies [9], and 47 and 48 meV in inelastic x-ray scattering [10]. The LO mode is resolved into two weak humps LO_1 and LO_2, around 525 − 542 cm^{-1} (65–67 meV) and 580 − 587 cm^{-1} (72–73 meV), respectively. To our knowledge, this could be one of the first Raman spectroscopic studies showing a clear anisotropy of the optical phonons in NiO. This observation is aided by the high resolution of the spectrometer due to the 2400 lines/grating as also a more diligent observation of the predicted phonon behavior

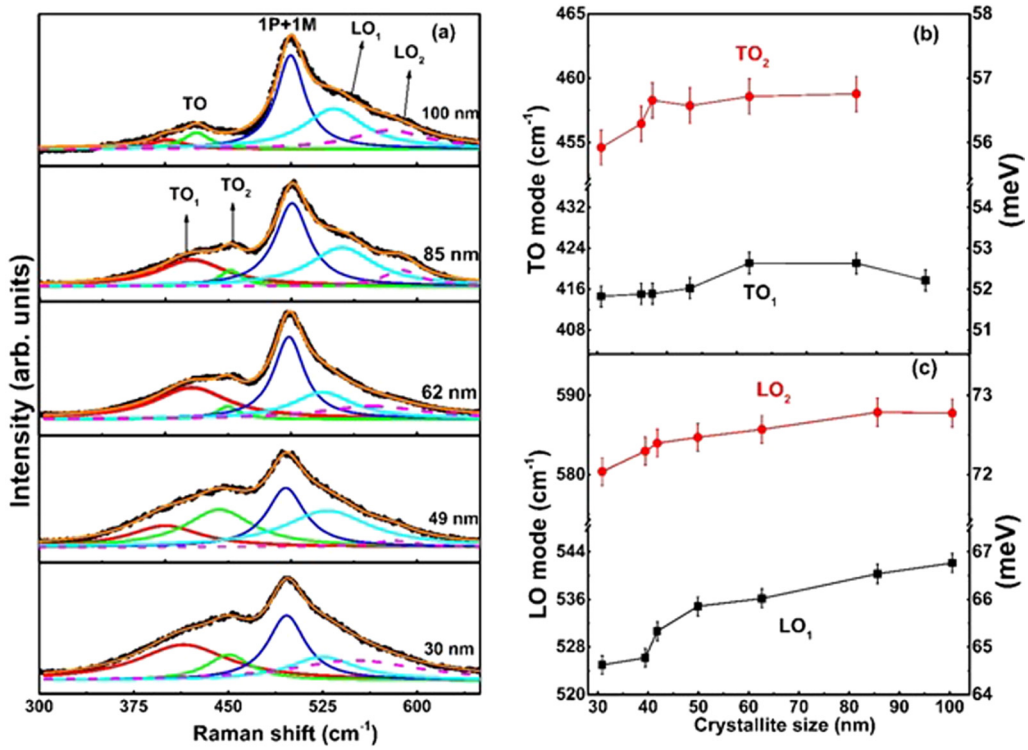

FIG. 4. (a) Deconvolution of the Raman spectra of NiO nanoparticles in the 300 to 650-cm^{-1} wave-number region. Variation of (b) TO_1 and TO_2 and (c) LO_1 and LO_2 modes with particle size. The solid lines in (b) and (c) are a guide to the eye.

motivated by previous theoretical predictions and experiments. The LO phonon energies are in reasonable agreement with previous studies, but the TO phonon energies in this work are consistently higher. The TO_1 mode however matches with the 413-cm^{-1} Raman mode reported by Aytan *et al.* [15] (their theoretical values were 360 and 367 cm^{-1}). Perhaps a more accurate inclusion of the Hubbard energy which accounts for strong electron correlations and upshifts the TO phonon [13] might better explain the experimental results for the NiO nanoparticles. It may be noted that there is a variation in the values of U in Refs. [11–13] in treating the lattice dynamics of NiO.

The TO phonon splitting was reported to arise only due to the coupling of the nearest-neighbor exchange interaction J_1 with the phonons and given by $\Delta_{TO} = \frac{d^2J1}{dQ_x\, Q_y}$, where J_1 is the nearest-neighbor coupling constant [12]. The coupling of the next-nearest-neighbor interaction J_2 was neglected because of its isotropic dependence on phonon displacement vs the anisotropic dependence for J_1. The predicted splitting matched well with the experimental results for MnO [9]. For NiO, the splitting was estimated to be 1.8 meV and lower than our experimental results and those of Ref. [9]. Therefore, the effect of J_2 merits consideration in the treatment based on exchange interaction considering its large magnitude for NiO (19.01 meV as compared to 0.89 meV for MnO and also being almost ten times stronger than the J_1 value of 1.37 meV in NiO). Further, the J_1 exchange is related with ferromagnetic ordering in NiO in contrast to the antiferromagnetic one in MnO. The treatment of the splitting in terms of the anisotropic polarization of the magnetic (Ni) and nonmagnetic (O) atoms [10], distinct from the exchange-interaction treatment of Ref. [12], could be coincidental in view of the similar magnitudes of the anisotropy constant and J_1 [6]. Floris *et al.* [13] predicted a similar magnitude of the splitting for the TO phonons, and further added that the different occupancy of the minority-spin d electrons states of (3 for MnO to 0 for NiO) explains the sign change of Δ_{TO}. They estimated the LO phonon by adding to the GGA+U Hamiltonian a nonanalytical term which depends on the dielectric constants and the Born effective charges. Our LO peak positions are in the range of predicted values.

The other feature in the Raman spectrum which is a probe of the magnetic-domain structure is the zone-boundary two-magnon scattering. We observe a redshift, broadening, and damping of the mode with a decrease in size. The 2M band shifts linearly from 1448 cm^{-1} (179.6 meV) to 1492 cm^{-1} (184.9 meV) for the particle size varying between 30 and 100 nm as illustrated in Fig. 5. A similar trend is observed for another set of nanoparticles formed by oxygen annealing (not shown). It may be mentioned that the smaller sizes (black color) have a higher Ni vacancy concentration compared to the larger size (green) as determined from energy-dispersive spectroscopy. In contrast, the 2M energies were reported to be the same for both black (nonstoichiometric) and green (stoichiometric) bulk NiO [20]. Gandhi *et al.* [26] reported it to be nearly constant for sizes between 75 and 416 nm in NiO nanowalls and for sizes between 31 and 56 nm in NiO nanoparticles, with an exponential variation in between 16.6 and 56 nm for the latter. Mironova-Ulmane *et al.* showed the 2M peak to be invariant in position and intensity for

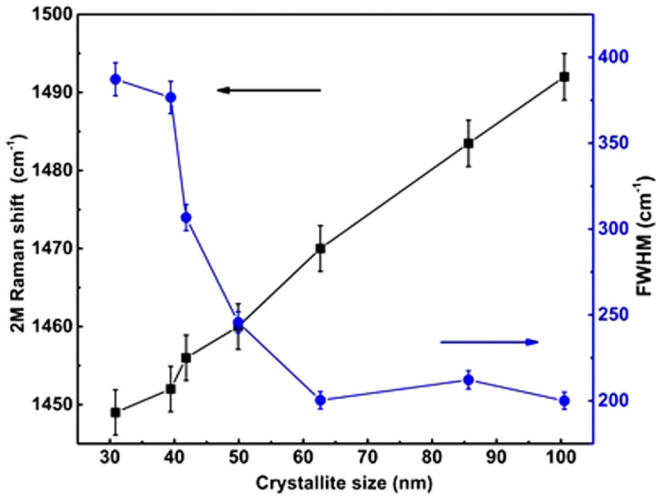

FIG. 5. Variation of 2M mode with crystallite size. The solid lines are a guide to the eye.

particle sizes between 13 and 23 nm [18]. A linear reduction in the 2M peak position and an increase in broadening was also reported with alloying of NiO with Mg and Ca [27,28] and attributed to the lowering of the local symmetry at the Ni^{2+} sites. However, while a breakdown of the symmetry in nanoparticles can also activate magnons additionally in the vicinity of the zone boundary, this alone cannot explain the large size-dependent shift. The incident laser power is another factor that influences the peak positions [29] and structural transformations [17,30]. This is particularly true in nanostructures where self-heating effects may arise due to their low thermal conductivity. Mironova-Ulmane *et al.* showed a softening of the 2M peak position and a reduction in its intensity for an increase in power from 0.1 to 1 mW. A further increase to 5 mW led to the disappearance of the 2M peak [18]. This process was reported to be reversible. Lacerda *et al.* [17] showed that increasing the laser power led to a softening of the magnon peak position and its disappearance above T_N, but a further increase in the laser power caused an increase in the local temperature above T_N and an irreversible structural transformation. The low laser power used in our measurements rules out heating effects on the 2M peak.

The magnetic configuration is, in general, determined by nearest- and next-nearest-neighbor exchange interactions, whose contribution to the energy of the 2M peak is determined by the spin-spin Heisenberg interaction $H = \sum_{NN} J_1 Si\, Sj + \sum_{NNN} J_2 Si Sj$, where the first term is the weaker ferromagnetic interactions connecting the 12 nearest neighbors and the second term corresponding to the superexchange interactions connecting each Ni to its six next-nearest neighbors along ⟨100⟩ directions is the dominant antiferromagnetic interaction. The magnitude of J_2 (∼19.01 meV) compared to J_1 (∼1.37 meV) often leads to a neglect of the latter when investigating the effect of exchange interactions on electronic and vibrational properties. Similarly, the contributions of anisotropy and dipolar interactions, being much smaller [6], are also neglected. The experimental values of J_1 and J_2 have been determined in neutron-scattering experiments [21] and other studies. The 2M Raman mode in bulk NiO reported at around 1460–1500 cm^{-1} was explained using the Heisenberg interaction [20,22].

The persistence of the 1P + 1M and the disappearance of the 2M with decreasing size agrees with the prediction [19] that the mechanisms for first- and second-order magnon scattering are different and also that the exchange mechanism is not operative for ferromagnets and therefore a two-magnon state is not observed for ferromagnetic nanoparticles. The size variation of 2M peak position is proposed to be due to the magnetic structure of nanoparticles being different from that of bulk materials. As proposed by Kodama *et al.* [1], the standard two-sublattice configuration magnetization used for explaining antiferromagnetism in bulk NiO would be replaced by a multisublattice configuration for nanoparticles. A consequence of the multisublattice model is the decrease in the value of S from 1 for bulk NiO and an increase in the number of sublattices from 2 to 8 in nanoparticles. Incorporating these conditions in the Heisenberg interaction could help explain the size variation of the 2M energy. The total exchange interaction also decreases for surface atoms in nanoparticles due to their lower coordination number. The damping and eventual disappearance of 2M with decreasing sizes correlates with the antiferromagnetic-ferromagnetic transformation observed in magnetic measurements. The 2M exhibits also exhibits unusually large linewidths varying between 200 and 400 cm^{-1} with the high-energy tail extending to well beyond 1800 cm^{-1}. Inclusion of both magnon-magnon and magnon-phonon interactions is necessary to explain both the energy and the line shape of the magnon energy [22].

The excitation wavelength dependence of the Raman spectrum provides further insights into the behavior of the 2M mode. A comparison of the Raman spectra in the near-resonance and off-resonance condition (done with excitation wavelengths of 325 and 514.5 nm) is shown in Fig. 6. The intensities of the 2M and 1P + 1M are suppressed near-resonance condition, while they are sizable for off-resonance. This is consistently observed for various NiO nanoparticles. A similar behavior for the 2M mode was observed by Aytan *et al.* [15] and a temperature-dependence study was used to elucidate the magnon-phonon interactions [15,17]. In general, light does not interact directly with the spin system. However, when the excitation photon energy is considerably smaller than the band gap, two-magnon scattering can occur due to exchange mechanisms. Chubukov and Frenkel [31] showed that the strength of the two-magnon Raman scattering shows a maximum away from the band gap, unlike phonons which exhibit resonances with the peak of the dielectric constant. Pressl *et al.* [25] measured the wavelength variation of the 2M mode and showed the 2M resonance to occur around 2.1 eV. In summary, both the zone-edge and zone-center magnons are seen to be influenced by the excitation wavelength, although they have different origins [19]. In order to verify the resonance behavior and understand the reasons thereof, more detailed wavelength-dependent studies are required and outside the scope of this work.

Distinct changes in the magnetic behavior as a function of particle size are illustrated in the *M-H* curves shown in Fig. 7,

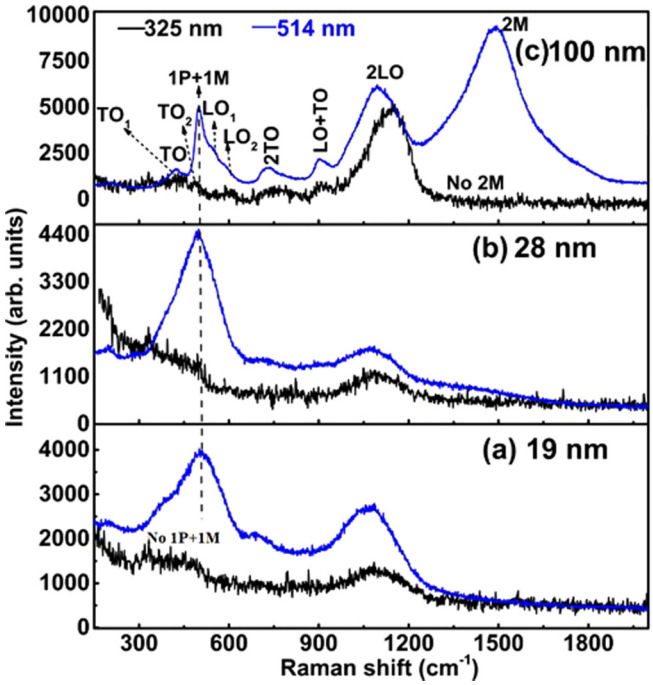

FIG. 6. Raman spectra of NiO nanoparticles at excitation wavelengths of 325 and 514. 5 nm. The 1P + 1M and 2M are absent for 325 nm.

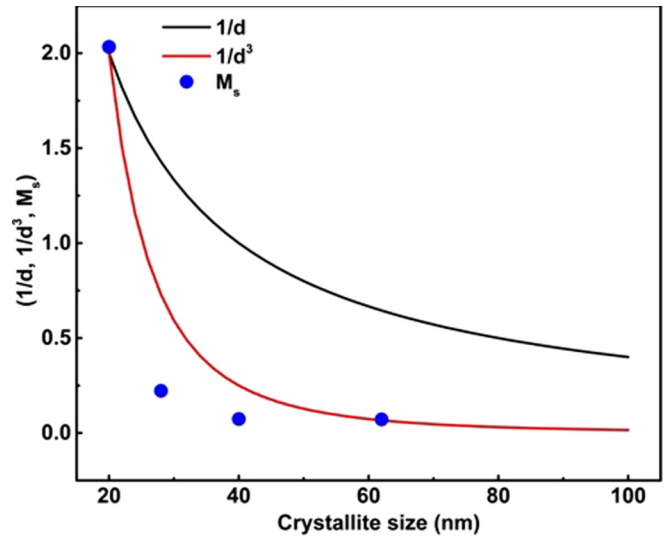

FIG. 8. Saturation magnetization (M_s, $1/d$, $1/d^3$) versus crystallite size of NiO.

as also reported in Refs. [32,33] for example. A clear hysteresis loop observed for low particle sizes is representative of ferromagnetic behavior, while a shifting of the hysteresis loop for large particle sizes indicates antiferromagnetic behavior. A small diamagnetic contribution is also seen above ∼10 000 Oe and could be a result of the Ni vacancy. The stoichiometry changes with annealing supports this observation. The samples of intermediate sizes exhibit a weak ferromagnetism. The saturation magnetization exhibits a distinct size dependence, increasing significantly from 0.07 emu/g for 2 nm size to 2.03 emu/g for 19 nm as shown in Fig. 8. The nature of the *M-H* loops and the extracted values of M_S showing a decrease of antiferromagnetic spin correlations and enhanced ferromagnetic fraction at small crystallite sizes can be correlated to changes in the Raman spectra. Further, this enhancement in M_S could be explained by the thermoinduced contribution to the magnetic moment of nanoparticles of antiferromagnetic materials [34] which also explains the vanishing antiferromagnetism for lower particle sizes. The thermoinduced magnetization is predominant at room temperature for antiferromagnetic materials with a size below a few nm and may be distinguished from other contributions, from its temperature and size dependence. The size dependence is proportional to d^{-3}, where d is the particle diameter, whereas the size dependence due to uncompensated spins is approximately proportional to d^{-1} and therefore expected to be smaller [35]. Figure 8 shows that the experimental values of the magnetization agree better with a d^{-3} dependence.

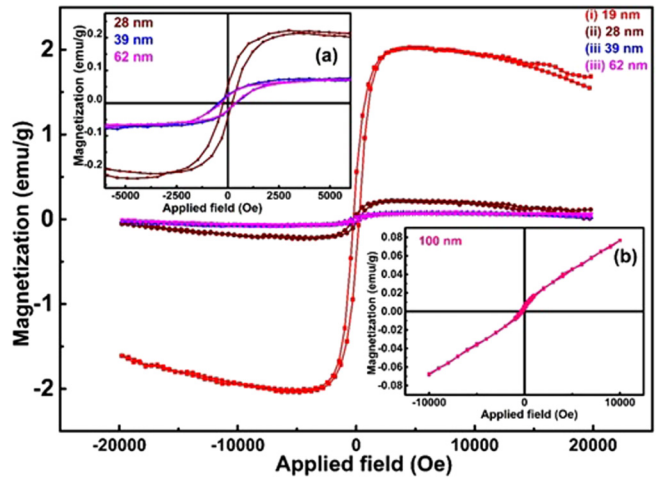

FIG. 7. Room-temperature *M-H* loops of NiO nanoparticles as a function of crystallite size. Inset (a) shows a clear hysteresis behavior and magnetic saturation at an applied field of 5000 Oe, and (b) shows the shifted hysteresis loop for 100-nm size.

IV. CONCLUSION

In conclusion, magnetic-order induced effects are manifested in the Raman spectrum of NiO. An anisotropy of about 5 meV in the TO and LO phonons and a remarkable softening of the 2M by about 50 cm^{-1} for particle sizes between 30 and 100 nm are observed. Further, the phonon plus magnon (1P + 1M) as well as the two-magnon (2M) modes show a stark wavelength dependence. High-resolution micro-Raman spectroscopy, with a higher sensitivity as compared to neutron scattering and allowing measurements on microscopic volumes, is a useful tool for the study of the magnetic structure of NiO nanoparticles. Further, the size variation of the magnetic behavior is understood from the thermoinduced magnetiza-

tion. Such studies are relevant for the applications of NiO in both ferromagnetic and antiferromagnetic spintronics. These observations may also encourage further studies of the lattice dynamics of strongly correlated NiO and also help understand the cumulative role of anisotropy, dipolar interactions, and exchange phenomena.

ACKNOWLEDGMENTS

N.B. acknowledges financial support from University Grants Commission, India for Junior Research Fellowship [Ref. No. 22/06/2014(i)EU-V]. The authors are also thankful to USIC Delhi University, DST-FIST, and National Physical Laboratory, CSIR, New Delhi for measurement facilities.

[1] R. H. Kodama, S. A. Makhlouf, and A. E. Berkowitz, Phys. Rev. Lett. **79**, 1393 (1997).

[2] I. Sugiyama, N. Shibata, Z. Wang, S. Kobayashi, T. Yamamoto, and Y. Ikuhara, Nat. Nanotechnol. **8**, 266 (2013).

[3] S. D. Tiwari and K. P. Rajeev, Phys. Rev. B. **72**, 104433 (2005).

[4] W. Reichardt, V. Wagner, and W. Kress, J. Phys. C: Solid State Phys. **8**, 3955(1975).

[5] R. A. Coy, C.W. Tompson, and E. Gürmen, Solid State Commun. **18**, 845 (1976).

[6] S. K. Agarwal, Solid State Commun. **29**, 197 (1979).

[7] M. D. Towler, N. L. Allan, N. M. Harrison, V. R. Saunders, W. C. Mackrodt, and E. Aprà, Phys. Rev. B **50**, 5041 (1994).

[8] S. Massidda, M. Posternak, A. Baldereschi, and R. Resta, Phys. Rev. Lett. **82**, 430 (1999).

[9] E. M. L. Chung, D. M. K. Paul, G. Balakrishnan, M. R. Lees, A. Ivanov, and M. Yethiraj, Phys. Rev. B. **68**, 140406(R) (2003).

[10] H. Uchiyama, S. Tsutsui, and A. Q. R. Baron, Phys. Rev. B **81**, 241103(R) (2010).

[11] S. Y. Savrasov and G. Kotliar, Phys. Rev. Lett. **90**, 056401 (2003).

[12] W. Luo, P. Zhang, and M. L. Cohen, Solid State Commun. **142**, 504 (2007).

[13] A. Floris, S. de Gironcoli, E. K. U. Gross, and M. Cococcioni, Phys. Rev. B **84**, 161102(R) (2011).

[14] Y. Wang, J. E. Saal, J.-J. Wang, A. Saengdeejing, S.-L. Shang, L.-Q. Chen, and Z.-K. Liu, Phys. Rev. B **82**, 081104(R) (2010).

[15] E. Aytan, B. Debnath, F. Kargar, Y. Barlas, M. M. Lacerda, J. X. Li, R. K. Lake, J. Shi, and A. A. Balandin, Appl. Phys. Lett. **111**, 252402 (2017).

[16] N. Mironova-Ulmane, A. Kuzmin, I. Steins, J. Grabis, I. Sildos, and M. Pärs, J. Phys. Conf. Ser. **93**, 012039 (2007).

[17] M. M. Lacerda, F. Kargar, E. Aytan, R. Samnakay, B. Debnath, J. X. Li, A. Khitun, R. K. Lake, J. Shi, and A. A. Balandin, Appl. Phys. Lett. **110**, 202406 (2017).

[18] N. Mironova-Ulmane, A. Kuzmin, I. Sildos, L. Puust, J. Grabis, and Latvian, J. Phys. Tech. Sci. **56**, 61 (2019).

[19] P. A. Fleury and R. Loudon, Phys. Rev. **166**, 514 (1968).

[20] R. E. Dietz, G. I. Parisot, and A. E. Meixner, Phys. Rev. B. **4**, 2302 (1971).

[21] M. T. Hutchings and E. J. Samuelsen, Phys. Rev. B **6**, 3447 (1972).

[22] M. G. Cottam and M. G. Cottam, Solid State Commun. **10**, 99 (1972).

[23] D. J. Lockwood, M. G. Cottam, and J. H. Baskey, J. Magn. Magn. Mater. **104–107**, 1053 (1992).

[24] M. J. Massey, N. H. Chen, J. W. Allen, and R., and Merlin, Phys. Rev. B **42**, 8776 (1990).

[25] M. Pressl, M. Mayer, P. Knoll, S. Lo, U. Hohenester, and E. Holzinger-Schweiger, J. Raman Spectrosc. **27**, 343 (1996).

[26] A. C. Gandhi, C. Y. Huang, C. Yang, T. Chan, C. L. Cheng, Y. R. Ma, and S. Wu, Nanoscale Res. Lett. **6**, 485 (2011); A. C. Gandhi, J. Pant, S. D. Pandit, S. K. Dalimbkar, T. S. Chan, C. L. Cheng, Y. R. Ma, and S. Y. Wu, J. Phys. Chem. C **117**, 18666 (2013).

[27] E. Cazzanelli, A. Kuzmin, N. Mironova-Ulmane, and G. Mariotto, Phys. Rev. B. **71**, 134415 (2005).

[28] E. F. Funkenbusch and B. C. Cornilsen, Solid State Commun. **40**, 707 (1981).

[29] K. A. Alim, V. A. Fonoberov, and A. A. Balandin, Appl. Phys. Lett., **86**, 053103 (2005); K. A. Alim, V. A. Fonoberov, M. Shamsa, and A. A. Balandin, J. Appl. Phys. **97**, 124313, (2005).

[30] B. Hadžić, B. Vasić, B. Matović, I. Kuryliszyn-Kudelska, W. Dobrowolski, M. Romčević, and N. Romčević, J. Raman Spectrosc. **49**, 817 (2018).

[31] A. V. Chubukov and D. M. Frenkel, Phys. Rev. B **52**, 9760 (1995).

[32] S. Thota and J. Kumar, J. Phys. Chem. Solids **68**, 1951 (2007).

[33] N. Mironova-Ulmane, A. Kuzmin, J. Grabis, I. Sildos, V. I. Voronin, I. F. Berger, and V. A. Kazantsev, Solid State Phenom. **168–169**, 341 (2011).

[34] S. Mørup and C. Frandsen, Phys. Rev. Lett. **92**, 217201 (2004).

[35] T. Richardson, D. I. Yiagas, B. Turk, K. Forster, and M. V. Twigg, J. Appl. Phys. **70**, 6977 (1991).